Mode filtering to reduce ultrasound speckle for feature extraction

A.N. Evans, PhD
M.S. Nixon, PhD, MIEE, CEng

Indexing terms: Feature extraction, Speckle filtering, Ultrasound imaging

Abstract: The authors investigate the use of filtering techniques to reduce speckle in ultrasound images, to improve their suitability for later feature extraction. The maximum likelihood estimator for a speckle corrupted image is shown to correspond to the statistical mode but this is difficult to determine for small populations, such as those contained by a filter mask. The truncated median filter approximates the mode by using the order of known image statistics and provides a fully automated image processing technique for speckle filtering. The filter's performance is established using a new quantitative evaluation scheme that closely considers the effect of filtering on edges, a key factor when applying features extraction in automated image interpretation. Application to *in vivo* and phantom test images shows that the truncated median filter provides clear images with strong edges, of quality exceeding that of other techniques. These benefits are confirmed by the application of feature extraction in arterial wall labelling.

1 Introduction

1.1 Speckle statistics

Speckle is multiplicative Rayleigh noise which degrades ultrasound images by concealing fine structures and reducing the signal to noise ratio (SNR). The theoretical aspects of ultrasound speckle have been studied by several authors including Wells [20] and Wagner [19]. Given an observed signal z which results from the multiplication of a signal component, m, and a noise component n, then

$$z = mn$$

The Rayleigh distribution is characterised by

$$f(z) = \begin{cases} \frac{z}{\sigma^2} \exp\left(\frac{-z^2}{2\sigma^2}\right) & \text{if } z > 0 \\ 0 & \text{otherwise} \end{cases}$$

Paper 1800K (E4, S9), first received 24th May and in revised form 23rd December 1994

A.N. Evans was with the Department of Electronics and Computer Science, University of Southampton and is now with the Department of Production Technology, Massey University, Private Bag 11222, Palmerston North, New Zealand.

M.S. Nixon is with the Department of Electronics and Computer Science, University of Southampton, Highfield, Southampton SO17 1BJ, United Kingdom

with mean $\sigma\sqrt{(\pi/2)}$ and variance $\sigma^2(2 - \pi/2)$. Kotropoulos and Pitas [10] have derived a maximum likelihood estimator for the underlying raw ultrasound signal, corrupted by noise of unity expected value, by maximising the conditional probability distribution function (PDF)

$$p\left(\frac{z}{m}\right) = \frac{1}{m}\left(\frac{z}{\sigma^2 m} \exp\left(\frac{-z^2}{2\sigma^2 m^2}\right)\right)$$

For a series of N observations, z_i ($i \in 1, N$), the joint conditional PDF can be expressed as a log-likelihood function

$$\ln\left(p_N\left(\frac{z}{m}\right)\right) = -2N \ln(\sigma) - 2N \ln(m) + \sum_{i=1}^{N} ln(z_i) + \frac{\sum_{i=1}^{N} z_i^2}{2\sigma^2 m^2}$$

for which a maximum likelihood estimator, m_{ml}, can be found setting the differentiation of the conditioned likelihood function $\partial p_N(z/m)/\partial m$ equal to zero, with solution

$$m_{ml} = \sqrt{\left(\frac{\sum_{i=1}^{N} z_i^2}{2\sigma^2 N}\right)}$$

This provides an estimate for a constant signal and in the presence of a random signal the maximum *a posteriori* estimate, formulated under the assumption that the underlying signal has a Maxwell distribution, can reduce to the maximum likelihood estimate for the constant signal [10]. It has further been shown that the maximum likelihood estimator for the displayed ultrasound image closely resembles that of the original signal [9].

As an alternative approach, the maximum of the Rayleigh distribution provides a value of the underlying signal consistent with the maximum likelihood estimator. Again we seek the distribution's maximum which, by differentiation, occurs at

$$\frac{\partial p(z)}{\partial z} = 0 = \exp\left(\frac{-z^2}{2\sigma^2}\right)\left(1 - \frac{z^2}{\sigma^2}\right)$$

and hence for a value

$$z = \sigma$$

The authors would like to thank T.K. Hames of Southend Hospital for his constructive advice and A.N. Evans gratefully acknowledges the research grant from SERC that made this work possible.

This identifies a value for the corrupted signal, z, to maximise the probability density function. This value of z is the statistical mode. Given a constant signal corrupted by Rayleigh noise, the mode of a set of observations then corresponds to the maximum likelihood estimator of the underlying signal. In addition, seeking the mode can accommodate deviations from the underlying theoretical models, such as nonlinearities and envelope smoothing, that are present in any practical ultrasound imaging system [18].

1.2 Other approaches

A statistical approach has not been used in many extant speckle reduction techniques which have been based on image compounding, on phase-based methods and on image filtering. Compounding techniques capitalise on speckle non-stationarity in different images to produce a single output image, and may be time, spatial or frequency based. Phase-based methods identify interference via the measured backscatter frequency and then remove it.

There are many established image processing techniques that can be used to reduce the noise in images, of which the median filter is arguably the most popular nonlinear method. This is because median filtering is well suited to the reduction of speckle-type structures. However, although the median filter can successfully remove speckle noise, it fails to sufficiently preserve the weak, diffuse edges that characterise ultrasound images, thus motivating the development of adaptive speckle filters [1, 12]. Other approaches such as Greiner *et al.* [6] have used techniques developed for synthetic aperture radar and translated them for ultrasound images. The ability to display the original image in tandem with the processed result is of importance to radiographers, who can interpret image features from the specular information, and is easily implemented with image processing techniques. None of these established techniques have been based on maximum likelihood principles. However, the earlier analysis indicates that the mode might be suitable as an estimate of the underlying distribution. We therefore seek to investigate the behaviour of the mode as an estimator in speckle corrupted ultrasound images.

There is a further advantage to seeking the mode which accrues from its performance as an image processing technique, mainly that it serves to reinforce edge data in images. This is advantageous if the speckle reduced image is to be used as an input for a further feature extraction stage, such as that in 3D arterial reconstruction [13] or in temporal tracking of anatomical structures [8], which rely on accurately locating the edges within the ultrasound image. In feature extraction where we are concerned not only with the diagnostic appearance of the image, but more importantly its suitability for automatic interpretation, then the performance of an estimator with edge reinforcement can prove important.

Subjective evaluation techniques, such as those of Loupas [11] and Crawford *et al.* [2], though useful for assessing clinical content of images, are of limited value when assessing the suitability of filtered images for later feature extraction since both qualitative and quantitative measures are required. A fundamental component of an objective evaluation scheme is the effect of a speckle reduction technique on the position and strength of edges present within the image. The Canny edge detector is used to evaluate this in conjunction with a phantom test image containing known edge detail, so that the effects of speckle reduction on perceived edge position can be assessed.

2 Speckle reduction methods

Speckle reduction techniques can be sub-divided into three classes: compounding, phase-based methods and filtering. Compounding techniques make use of the non-stationarity of speckle to produce a single, improved output image from several input images. Input images may be obtained by several methods, for example by direct averaging of a time series of images as implemented on a number of scanners. Compounding may also be spatial, such as weighted spatial averaging [15], or by using a two-dimensional arrays of transducers [5]. Frequency compounding uses varying frequency to obtain a set of images. This may be simply produced by using different centre frequencies, or by a more complex method, such as frequency diversity where the channels of filtered input data are envelope-detected and then compounded. Spatial and frequency compounding has also been combined to improve speckle reduction [17].

Phase-based methods use the instantaneous frequency of backscatter echo to identify the presence of destructive interference. Once located, the speckle may be removed by several techniques including frequency differencing or the local frequency diversity [4]. Alterntively the speckle can be corrected in the complex z-domain, in which signal amplitude and phase can be manipulated simultaneously [7].

There are many established image processing techniques, such as the median filter, that can be used to reduce the noise in images. The wide variation of image statistics and low contrast displayed by ultrasound images has motivated the development of adaptive filters, such as the adaptive weighted median filter of Loupas *et al.* [12] and the unsharp masking filter of Bamber and Daft [1], that exhibit increased performance at edges whilst retaining a strong smoothing action in speckle affected regions. These filters use local image statistics to vary the output between the original value and the mean or median of a local region. In both cases the ratio of the local mean to the local variance controls the proportion of each, with the output tending towards the original value where the ratio is low, i.e. at an edge, thus improving the performance of the filter at discontinuities.

The weighted median filter uses weighting coefficients, denoted $w_1, w_2, \ldots, w_N$, to repeat the corresponding terms of the ranked pixel intensity values, $\{f_1, f_2, \ldots, f_N\}$, w_i times to form an extended sequence $\{w_1 f_1, w_2 f_2, \ldots, w_N f_N\}$. For a square window with sides of length $2K + 1$ the weight coefficient $w_{i,j}$ at position (i, j) is given by

$$w_{i,j} = [W_{(K+1,K+1)} - cd\sigma^2/\bar{x}]$$

where $W_{(K+1,K+1)}$ is the central weight and [ ] denotes the nearest integer to the term inside the brackets or zero if the result of the addition within them is negative; c is a scaling constant and d is the distance of the point from the centre of the window. The local mean is denoted by $\bar{x}$ and the local variance by σ^2, both taken over the area of the mask, $W_{(K+1,K+1)}$ and c were set so that in an area consisting solely of speckle, where the ratio of variance to mean intensity, $\sigma^2/\bar{x}$, is low, the filter performs as a median filter but at an edge, where $\sigma^2/\bar{x}$ is high, the output is biased towards the original intensity value.

The unsharp masking filter is an adaptive mean-based filter and uses the measure of similarity, p, given by the ratio of the variance to the mean within the filter

window, to control a constant k such that $0 \leqslant k \leqslant 1$ by

$$k = (gp - \bar{p}_s)/p$$

where $\bar{p}_s$ is the mean value of p for a local area of an image that is considered to consist of fully developed speckle. The constant g is a scaling factor that allows the aggressiveness of the smoothing to be adjusted. By varying the constant k between zero and one, we can adaptively adjust the output, $\hat{x}$, between the original intensity (x) and the local mean ($\bar{x}$) by

$$\hat{x} = \bar{x} + k(x - \bar{x})$$

The value of g is chosen to ensure that, for a given image, k is always less than one, thus avoiding edge enhancement. A suitable value for $\bar{p}_s$ is the average of ten measurements in an area considered to consist solely to speckle on a dark background. These adaptive filters have a high computational cost and require prior choice of controlling parameters; in practice this often necessitates an initial pass of the filter over the image.

This paper introduces the use of Davies's truncated median filter [3] to filter ultrasound images, contrasting the results achieved with those of contemporary speckle filters. The filters used for comparison were a standard median filter, the adaptive median filter and the adaptive unsharp masking filter. The aim was to determine whether a simple non-adaptive filter that, by estimating the mode of the underlying distribution and hence approximating a maximum likelihood estimator, can achieve results acceptable for a further computer vision stage with a fully automatic implementaton and reduced computational complexity compared with extant filters.

3 Truncated median filter

The truncated median filter was first proposed by Davies [3] and approximates to a modal filter. The most frequent value in any distribution is the mode, but the difficulty of determining the mode of a small population has meant that whilst the median filter enjoys great popularity the modal filter has largely been ignored. Near edges, the modal filter will suppress noise where little is present, or enhance the edge in the case of high noise; this enhancement is achieved by a nondistorting 'crispening' operation. When directly on an edge the mode can be either of two peaks as the population is essentially bimodal and this can result in rather coarse decisions being taken. The mode thus appears to offer an improvement over the median filter near to edges but may give erratic results when directly on the edge.

The ranking order of the mode, median and mean can be used to estimate the mode for many distributions, including those of ultrasound images. Fig. 1 illustrates

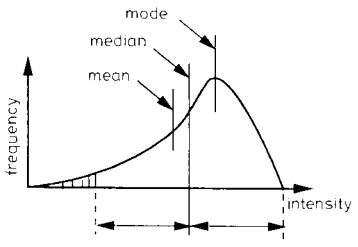

Fig. 1 *Normal order of mean, mode and median in a unimodal distribution and method of truncation*

that if the median is moved away from the mean then it will approximate to the mode. To move the median, Davies proposed to truncate the original frequency distribution graph so that the median bisects the range of distributions and a new median value found that is closer to the mode. This process is iterative, each pass of the filter moving the truncated median output further towards the mode, although in practice one pass has been found to be sufficient. Additionally if the filter is applied only once, the output errs towards the median thus overcoming the problem of the mode being too harsh at edges, as the output intensity value is not restricted to either of the two peaks in the intensity histogram. Fig. 2 illustrates this point for a bimodal distribution, showing the ideal truncation point and the actual

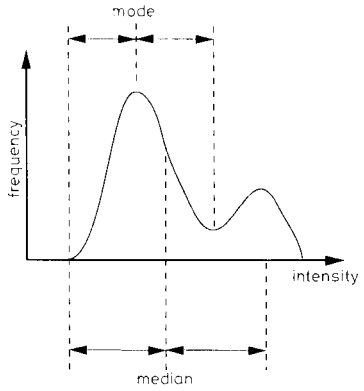

Fig. 2 *Bimodal distribution showing ideal truncation point (above) and actual truncation point (below)*

one, which lies to the median side of the mode. The truncated median filter therefore supplies a result equivalent to the mode of a distribution when away from and close to an edge but retains more median information when directly on an edge. This is a filtering action similar to that of adaptive filters but, by providing the mode, is consistent with the maximum likelihood estimator for a contant signal described earlier.

4 Experimental results

All filters were applied to *in vivo* and phantom test images. With all filters there is a trade-off between mask size and computation time; for the results presented in this paper a mask size of 9 × 9 was used for the *in vivo* images and of 7 × 7 for the phantom test image, in order to preserve fine detail. There has been study on the optimal window shape and size [16] but here all filters have been implemented with square windows, enabling comparison with the results of other methods. To evaluate the suitability of speckle reduction as an image primer for automatic interpretation an approach has been adopted that encompasses three classes of measures. The first is a subjective appraisal of the resulting images, which is then complemented by quantitative measures. Finally, an edge detector is applied to determine the effect of the filtering methods on the edges present within the image. The application of a two-stage feature extraction technique is used to illustrate the advantages the truncated median filter confers to ultrasound images.

Quantitative measures that can be used include the contrast to speckle ratio (CSR) of Patterson and Foster

[14], a measure of the observer's ability to observe a void or dark area against a background of speckle, defined as

$$\mathrm{CSR} = \frac{\bar{x}_0 - \bar{x}_i}{(\sigma_0^2 + \sigma_i^2)^{1/2}}$$

where $\bar{x}_i$ and σ_i^2 are the average signal value and the variance, respectively, inside the void and $\bar{x}_0$ and σ_0^2 are those outside the region. The local SNR is given by

$$\mathrm{SNR} = \frac{\bar{x}}{\sigma}$$

where $\bar{x}$ and σ denote mean and standard deviation respectively, measures of the amount of speckle present. Both the CSR and SNR were calculated over a 9×9 region, matching the filter mask size.

The design criteria and relative computational simplicity motivated the choice of the Canny edge detector for this research. By applying the Canny edge detector to filtered *in vivo* images and comparing the results with edges detected by the eye, the amount of edge preservation can be estimated. However, as we do not know what edges should be present and their exact position, this is of limited use. To this end, a circular pipe in a water bath, modelling an artery, was used as a phantom artery providing a real B-scan image, with all the limitations of the imaging system, containing an object of known size and shape. The pipe used was hard plastic, 250 mm long, 28 mm in diameter and 1.8 mm thick. With an ideal imaging system the B-scan image would contain two concentric circles corresponding to the inner and outer edges of the pipe. The actual image only approximates to this, but as the precise position of the edges is known this gives a standard to compare the filtered results with.

All images are 256×256 pixels with 256 grey levels. The phantom image and *in vivo* scan of the carotid artery were from an Aloka ASU-32WL Sector Scanner, digitised via an Imaging Technology Inc. ITI100 framestore hosted by a DEC μVAX II minicomputer.

4.1 In vivo test image

Figs. 3*a* to *e* present the original and filtered images of an *in vivo* scan if the carotid artery. Cosmetic improvement to the original image is achieved by all the filtering techniques although the edge blurring by the unsharp masking filter can be observed at the artery/tissue junction in Fig. 3*e*. In the median and adaptive median filtered images the edges around the artery are clearly defined with the strongest edge being displayed by the truncated median filter. The adaptive weighted filter clearly preserves features best and has been able to highlight small structures removed by other techniques, see for example the tissue interface in the upper left of Fig. 3*d*, which can be identified in the original image Fig. 3*a*.

The CSR and SNR were used to interpret the results, see Table 1. Here the centre of the artery provides the void average signal and variance ($\bar{x}_i$ and σ_i^2) for the CSR and an area consisting solely of speckle was used for $\bar{x}_0$ and σ_0^2. Speckled regions were used to calculate the SNR away from edges and the SNR at an edge was found at the tissue/artery boundary; at edges, a small change in the SNR indicates edge preservation. The unsharp masking filter consistently offered the smallest improvement in the CSR and SNR away from an edge and also showed the largest improvement in SNR at an edge, indicating the greatest edge modification. The CSR and SNR away from an edge are improved by 21.0 dB and 20.2 dB respectively by both the median and adaptive median filters, with the truncated median filter offering a slightly lower improvement in each case. After the unsharp masking filter, the median filter preserves less edge information (i.e. the greatest change in the SNR at an edge) then the truncated median filter and the adaptive weighted filter produces the best edge preservation, with virtually no change to the SNR.

Table 1: CSR and SNR of in vivo image

Filter type	Median	Truncated median	Adaptive weighted	Unsharp masking
CSR	18.3	15.3	18.3	10.5
Improvement (dB)	21.0	19.4	21.0	16.2
SNR on edge	1.63	1.26	1.37	2.31
Improvement (dB)	1.5	−0.7	−0.03	4.6
SNR off edge	73.7	62.9	73.7	44.6
Improvement (dB)	20.2	18.9	20.2	15.9

The ideal edge model is not known, but by observation of the Canny edge-detected images in Figs. 3*f* to *i*, conclusions can be drawn about the edge preserving properties of the filters. The adaptive weighted and truncated median filters have preserved more complete edges than the other techiques; for example the detail to the left of the artery in the Figs. 3*g* and *h* which is not present in the other filtered images, though clearly present in the original image. Those edges produced by the truncated median filter are strongly defined and continuous, comparing favourably with the median and adaptive median filters. Fewest edges are determined by the unsharp masking filter, Fig. 3*i*, and those that can be seen are rough and unsubstantial.

4.2 Phantom test image

The edge detected phantom images overlayed with the edges expected from an ideal imaging system are shown in Fig. 4. A close coupling between ideal and actual results is achieved, although the result of the unsharp masking filer, Fig. 4*d*, shows edges due to speckle that have been removed by the other techniques, illustrating the disadvantage of mean-based filtering.

To quantify how close the resulting images are to the overlayed image, the ratio of the number of edge points that correspond to points in the ideal edge to the total number of edge points was taken for each edge detected filtered image, rows two and three of Table 2. The truncated median technique shows the highest percentage of matching points, then the median filter with performance just better than that of the adaptive weighted median filter. The unsharp masking filter performs considerably worse than the other three methods but still offers a threefold improvement on the original, unprocessed

Table 2: Ratio of number of edge points matching ideal edge to total number of edge points for phantom test object

Filter type	Median	Truncated median	Adaptive weighted	Unsharp masking
Number of edge points found	236	217	221	467
Exact match (%)	25.8	29.0	25.3	12.6
Improvement (dB)	14.43	15.44	14.26	8.20
Nearest neighbour (%)	66.1	67.3	67.0	34.0
Improvement (dB)	13.86	14.02	13.97	8.09

image. However, an exact match is very precise and gives no credit to techiques that produce edge points close to, but not exactly on, the ideal edge points. By defining a margin of error, a match is deemed to occur if an edge point coincides with any of the points adjacent to the ideal edge points, giving the figures in rows four and five of Table 2. The truncated median filter still produces the highest ratio, but the adaptive weighted median shows an improvement on the median technique, which conforms with expectations. The unsharp masking filter's result is half that of the median-based methods and double that of the original image. A high ratio is analogous to improved SNR and CSR, showing preservation of the true edge points (the signal) and removal of false edge points caused by noise. The total number of edge points found by each method, row one of Table 2, indicate that the filters are capable of making this distinction.

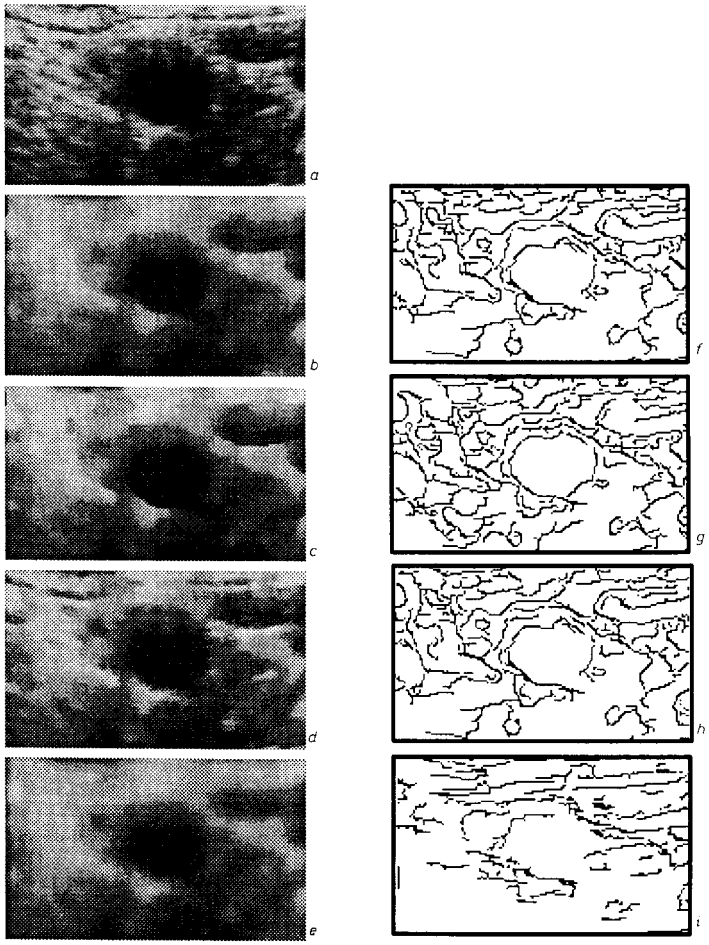

Fig. 3 *In vivo images*
a Original
b Median filtered
c Truncated median filtered
d Adaptive weighted median filtered
e Unsharp masking filtered
f–i Corresponding edge detected images

4.3 Feature extraction stage

Edge detection is a process of low-level or primary feature extraction. A common paradigm for automatic image interpretation is to group data derived from an edge detection process using a more sophisticated feature extraction technique. To illustrate the advantages that filtering can confer to automatic feature extraction, the filtering techniques have been incorporated within a package which provides a three-dinensional model of an artery by using noninvasive ultrasound [13]. This technique is based on developing the model from a series of cross-sectional scans; the processing sequence determines the arterial wall data in each ultrasound slice, which is then used to provide the 3D model. The operator first indicates the position of the artery in the image, marking a region of interest for locating arterial wall data in each transverse scan. The remainder of the processing is automatic. In order to handle not only the speckle, but also the discontinuities and occlusions present in ultrasound images, a two-stage technique was developed which first locates an ellipse and then labels edge data as arterial wall by examining deviation from the ellipse's perimeter. The ellipse is a development of the earlier use of a circle

and allows interpolation when data is absent within specified bounds. The artery is then reconstructed using a voxel-based solid model via first-order interpolation between the slices of arterial wall data. No filtering was used in the original system since its effect on the accuracy of edge data was not known.

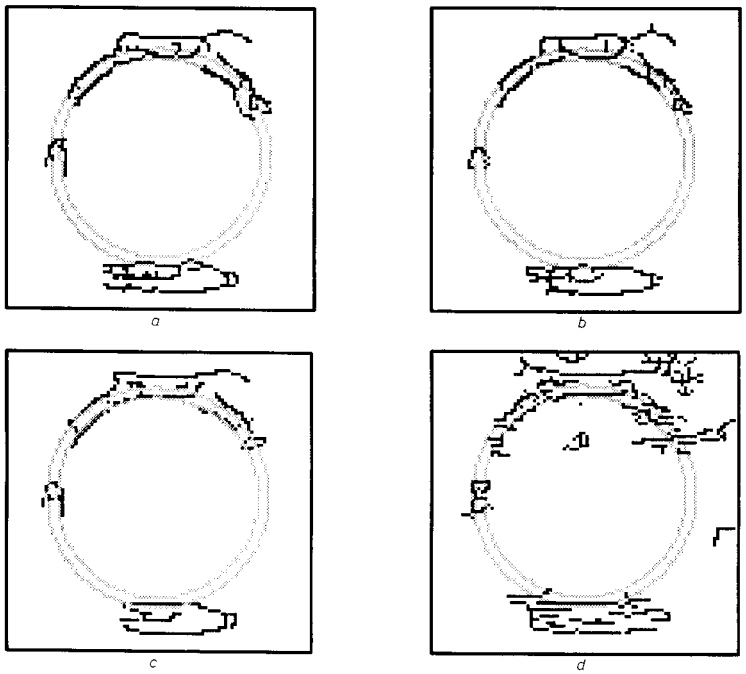

Fig. 4 *Filtered phantom images edge detected (black) and ideal image edge detected (grey)*
a Median *b* Truncated median *c* Adaptive weighted *d* Unsharp masking

The two-stage technique first determines an ellipse by using the Hough transform. This is an evidence-gathering technique which provides a result equivalent to template matching, but faster. its main attributes are that it performs well in noisy situations and it can handle occlusions and discontinuities and is, hence, eminently suited to application in ultrasound images. Edge data is then labelled as arterial wall by analysing deviation from the ellipse in a radial scan. Should it be within this range then it is labelled as wall data but when the closest edge data is beyond the specified range, or absent, then the ellipse selected by the Hough transform is used to infill for the missing data.

Filtering can improve both stages of the two-stage technique. The quality of the arterial wall data depends greatly on the quality of the edge data and so filtering would aim to improve the quality of the result. As the evidence gathered by the Hough transform is also based on edge data, if the data contains fewer points associated with speckle then the Hough transform can use data pertinent to the arterial wall alone, making this stage more robust.

The results of the two-stage arterial wall extraction technique are shown in Fig. 5 where the processing of the region of interest shows labelled arterial wall (in black) superimposed on grey level edge data. Fig. 5*a* is the result when applied to the raw, unfiltered image of Fig. 3*a*. This has three main regions of interest. In the left of the artery the edge data matched well to the detected ellipse and this has been labelled as arterial wall. The right of the artery contained poor edge data within the region associated with arterial wall and the ellipse was then used to infill for the missing data. The top of the artery shows the effects of fragmentary edge data associated with the unfiltered image. The circle from which the edge data is labelled bisects two fragmentary edge regions. Since the edge data is not solid this is reflected in the labelled arterial wall. This clearly reduces the quality of the result and appears as a discontinuous region in the 3D model.

Fig. 5*b* shows the result of the adaptive weighted median filter. In this the edge data is much more solid and the quality of the result is improved greatly. There is still some deviation from the edge contour at the top of the image and this is due to absent arterial wall data with the presence of a strong edge (attributable to tissue) in the near background. The truncated median filter brings the best performance, Fig. 5*c*. Its effect is to provide substantial and robust edge data and this can be seen at the top of the artery in comparison with Figs. 5*a* and *b*.

The result of the Hough transform is the best ellipse matching the edge data. One such result (that for the truncated median filter of Fig. 3*c*) is shown in Fig. 6, where the ellipse can be seen to match the arterial wall well. The major variation in the ellipse determined from the original and the filtered images was in the eccentricity. This was due to difference in quality of the edge data in the filtered images. This can be seen in the similarity between the sections of ellipse used to infill for missing data in the right of the artery in Figs. 5*a* and *b* where only very slight eccentricity of the ellipse is apparent. The centre co-ordinates of the detected ellipse varied at most by ± 1 pixel.

The use of the truncated median filter has then provided a better quality result together with a more robust

implementation. Both of these advantages are associated with the improvement in edge data derived from the filtered image which contributes greatly to improving the quality of the extracted features.

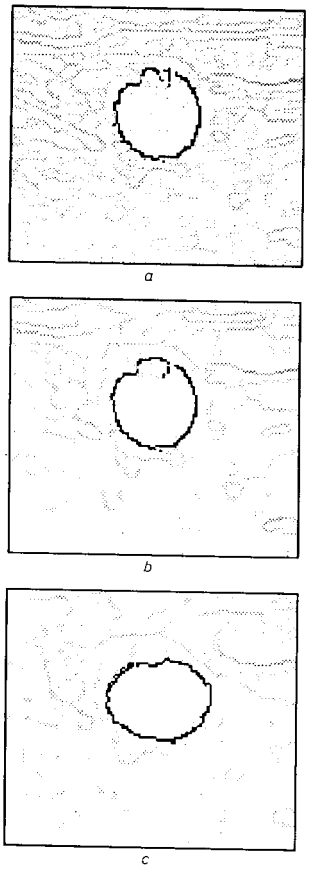

Fig. 5 *Feature extraction applied to:*
a Original image
b Adaptive weighted median filtered image
c Truncated median filtered image

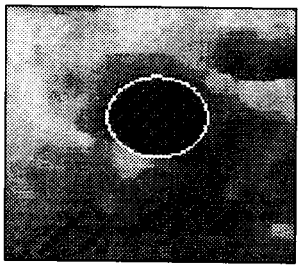

Fig. 6 *Result of Hough Transform for truncated median filtered image of Fig. 3c*

4.4 Processing times

The relative processing time for each technique, implemented in software on a DEC μVAX II minicomputer hosting an Imaging Technology Inc. ITI100 framestore, is used as a measure for comparison, see Table 3. Although these figures are obviously implementation dependent, relying on the hardware configuration, programming language nuances etc, it can be seen that the median and truncated median filters operate at a similar speed while the adaptive weighted median filter's complex nature is reflected in its long processing time.

Table 3: CPU times for filtering techniques

Filter type	Median	Truncated median	Adaptive weighted	Unsharp masking
Relative processing time	8.6	8.7	18.0	1

5 Conclusions

The use of speckle filtering techniques as image primers for a computer vision stage has been investigated. The mode is equivalent to a maximum likelihood estimator and is implemented by using the truncated median filter. Results have been assessed in comparison with contemporaneous techiques and the major advantages of the truncated median filter for ultrasound image processing are a better performance for later feature extraction with an automatic implementation, without any need for the user to specify controlling parameters.

In order to investigate the result of the truncated median filter in comparison with other techniques, a quantitative evaluation scheme has been proposed, based on the use of *in vivo* and phantom test images, objective measurements and the application of an edge detector. The use of a phantom to model the carotid artery provided an exact basis for comparison of filtered edge data with edge data derived from the raw images.

The result of the truncated median filter on an *in vivo* image surpasses that of the median filter and the adaptive unsharp masking filter, highlighting the deficiencies of mean-based filtering, and is comparable with that of the adaptive weighted median filter but without an excessive computational penalty. The phantom test image results confirm the superior edge-preserving properties of the truncated median filter to the median and unsharp masking filters. Application of a two-stage feature extraction method for arterial wall labelling demonstrates the advantages of using a speckle reduction technique before a further computer vision stage.

The truncated median filter has been found to offer an acceptable performance, with a fully automated implementation, producing images with well defined, continuous edges and therefore appears very suited to become part of the stock of tools for speckle reduction for enhanced ultrasound image analysis.

6 References

1 BAMBER, J.C., and DAFT, C.: 'Adaptive filtering for reduction of speckle in ultrasonic pulse-echo images', *Ultrasonics*, 1986, **24**, (1), pp. 41–44
2 CRAWFORD, D.C., COSGROVE, D.O., TOHNO, E., SVENSSON, W.E., AL-MURRANI, B., BELL, D.S., STEPNIEWSKA, K., and BAMBER, J.C.: 'Visual impact of adaptive speckle reduction on US B-mode images', *Radiology*, 1992, **183**, pp. 555–561
3 DAVIES, E.R.: 'On the noise suppression and image enhancement characteristics of the median, truncated median and mode filters', *Pattern Recog. Lett.*, 1988, **7**, (2), pp. 87–97
4 CATENBY, J.C., HODDINOTT, J.C., and LEEMAN, S.: 'Phasing out speckle', *Physics in Medicine and Biology*, 1989, **34**, (11), pp. 1683–1689
5 GIESEY, J.J.: 'Speckle reduction in pulse-echo ultrasonic imaging using a two-dimensional receiving array', *IEEE Trans. Ultrasonics, Ferroelectrics and Frequency Control*, 1992, **39**, (2), pp. 167–173

6 GREINER, T., LOIZOU, C., PANDIT, M., MAURUSCHAT, J., and ALBERT, F.W.: 'Speckle reduction in ultrasonic imaging for medical applications'. ICASSP, IEEE, 1991, pp. 2293–2296
7 HEALEY, A.J., LEEMAN, S., and FORSBURG, S.: 'Turning off speckle', *Acoustical Imaging*, 1992, **19,** pp. 433–437
8 HERLIN, I., and AYACHE, N.: 'Feature extraction and analysis methods for sequences of ultrasound images', *Image and Vision Computing*, 1992, **10,** (10), pp. 673–682
9 KOTROPOULOS, C., MAGNISALIS, X., PITAS, I., and STRINTZIS, M.G.: 'Nonlinear ultrasonic image processing based on signal-adaptive filters and self-organizing neural networks', *IEEE Trans. on Image Proc.*, 1994, **3,** (1), pp. 65–77
10 KOTROPOULOS, C., and PITAS, I.: 'Optimum nonlinear signal detection and estimation in the presence of ultrasonic speckle', *Ultrasonic Imaging*, 1992, **14,** (3), pp. 249–275
11 LOUPAS, T., ALLAN, P.L., and McDICKEN, W.N.: 'Clinical evaluation of a digital signal processing device for real-time speckle suppression in medical ultrasonics', *British J. Radiology*, August 1989, **62,** pp. 761–764
12 LOUPAS, T., McDICKEN, W.N., and ALLAN, P.L.: 'An adaptive weighted median filter for speckle suppression in medical ultrasound images', *IEEE Trans. Circuits and Systems*, 1989, **36,** (1), pp. 129–135
13 NIXON, M.S., and HAMES, T.K.: 'New technique for 3D artery modelling by noninvasive ultrasound', *IEE Proc. I*, 1993, **140,** (1), pp. 86–94
14 PATTERSON, M.S., and FOSTER, F.S.: 'The improvement and quantitative assessment of B-mode images produced by array/cone hybrid', *Ultrasonic Imaging*, 1983, **5,** pp. 195–213
15 SHANKAR, P.M.: 'Speckle reduction in ultrasound B-scans using weighted averaging in spatial compounding', *IEEE Trans. Ultrasonics, Ferroelectrics and Frequency Control*, 1986, **33,** (6), pp. 754–758
16 SMITH, S.W., WAGNER, R.W., SANDRIK, J.M., and LOPEZ, H.: 'Low contrast detectability and contrast detail analysis in medical ultrasound', *IEEE Trans. Sonics and Ultrasonics*, 1983, **30,** (3), pp. 164–173
17 TRAHEY, G.E., ALLISON, A.W., SMITH, S.W., and VON RAMM, O.T.: 'Speckle reduction achievable by spatial compounding and frequency compounding: experimental results and implications for target detectability', *in* SPIE Int. Symp. Pattern Recognition and Acoustical Imaging, 1987, **768,** pp. 185–192
18 WAAG, R.C., DEMCZAR, B.A., and CASE, T.J.: 'Nonlinear receiver compression effects on the amplitude distribution of backscattered ultrasonic signals', *IEEE Trans. Biomedical Engineering*, 1991, **38,** (7), pp. 628–633
19 WAGNER, R.F., SMITH, S.W., SANDRIK, J.M., and LOPEZ, H.: 'Statistics of speckle in ultrasound B-scans', *IEEE Trans. Sonics and Ultrasonics*, 1983, **30,** (3), pp. 156–163
20 WELLS, P.N.T., and HALLIWELL, M.: 'Speckle in ultrasonic imaging', *Ultrasonics*, 1981, **19,** (5), pp. 225–229